Available online at www.sciencedirect.com
SCIENCE DIRECT®
Medical Image Analysis 8 (2004) 447–464
MEDICAL IMAGE ANALYSIS
www.elsevier.com/locate/media

Strategies for brain shift evaluation

Peter Hastreiter [a,b,*], Christof Rezk-Salama [b], Grzegorz Soza [a,b], Michael Bauer [b], Günther Greiner [b], Rudolf Fahlbusch [c], Oliver Ganslandt [c], Christopher Nimsky [c]

[a] Neurocenter, Department of Neurosurgery, University of Erlangen-Nuremberg, Schwabachanlage 6, D-91054 Erlangen, Germany
[b] Computer Graphics Group, University of Erlangen-Nuremberg, Am Weichselgarten 9, 91058 Erlangen, Germany
[c] Department of Neurosurgery, University of Erlangen-Nuremberg, Schwabachanlage 6, 91054 Erlangen, Germany

Received 9 September 2003; received in revised form 26 January 2004; accepted 18 February 2004
Available online 23 April 2004

Abstract

For the analysis of the brain shift phenomenon different strategies were applied. In 32 glioma cases pre- and intraoperative MR datasets were acquired in order to evaluate the maximum displacement of the brain surface and the deep tumor margin. After rigid registration using the software of the neuronavigation system, a direct comparison was made with 2D- and 3D visualizations. As a result, a great variability of the brain shift was observed ranging up to 24 mm for cortical displacement and exceeding 3 mm for the deep tumor margin in 66% of all cases. Following intraoperative imaging the neuronavigation system was updated in eight cases providing reliable guidance. For a more comprehensive analysis a voxel-based nonlinear registration was applied. Aiming at improved speed of alignment we performed all interpolation operations with 3D texture mapping based on OpenGL functions supported in graphics hardware. Further acceleration was achieved with an adaptive refinement of the underlying control point grid focusing on the main deformation areas. For a quick overview the registered datasets were evaluated with different 3D visualization approaches. Finally, the results were compared to the initial measurements contributing to a better understanding of the brain shift phenomenon. Overall, the experiments clearly demonstrate that deformations of the brain surface and deeper brain structures are uncorrelated.

Keywords: Brain shift; Intraoperative MRI; Registration; Graphics hardware

1. Introduction

An increasing number of operations in brain surgery are performed with neuronavigation systems which improve spatial orientation, both while planning and carrying out surgical procedures. As an advantage of this strategy the surgical approach and the extent of lesions are defined more precisely. The basis of such systems are preoperatively acquired image data of different modalities such as computed tomography (CT) or magnetic resonance imaging (MRI). After identifying corresponding landmarks within the virtual space of the image data and the physical space of the patient, a registration is performed for the correlation of structures of the two spaces. In consequence, the physical location of surgical tools is mapped onto their corresponding position within the image data providing image guided orientation. Additionally, selected structures delineated within the image data are blended onto the patient using semi-transparent mirrors of modern operation microscopes (heads-up displays). Neuronavigation systems are most often applied in cases of tumors and angiomas located within eloquent areas of the brain. Furthermore, they are most useful for interventional therapy, surgery near the skull base and the sella region, biopsies and surgery for pharmacoresistant epilepsy.

The overall navigational accuracy of frameless stereotactic systems ranges between 1 and 2 mm (Kaus et al., 1997) and is thus in the order of magnitude of frame based systems (Maciunas et al., 1994). Mainly, it

* Corresponding author. Tel.: +49-9131-8534261; fax: +49-9131-8534271.
E-mail address: peter.hastreiter@neurozentrum.imed.uni-erlangen.de (P. Hastreiter).
URL: http://www9.informatik.uni-erlangen.de/Persons/Hastreiter/.

1361-8415/$ - see front matter © 2004 Elsevier B.V. All rights reserved.
doi:10.1016/j.media.2004.02.001

is composed of a technical error caused by the navigation system and an error resulting from the application. The latter is dominated by the precision of the imaging system (e.g., pixel size, image distortion) and the quality of the applied registration procedure. Overall, the total error of the whole system is most important for the application in surgical procedures. As a major drawback the precision of such systems is further influenced by two intraoperative events. This is the positional shift caused by moving the patient out of the coordinate system due to imprecise fixation. However, the most significant factor is a severe deformation of the brain occurring during neurosurgical operations on the opened skull. In fact, this deformation is an order of magnitude greater than other sources of errors in surgical navigation systems, which makes it the dominant contributor to the total error of the surgical navigation system.

This phenomenon known as *brain shift* is caused by various interacting factors such as the characteristics of tissue, the intraoperative positioning of the patient, the drainage of cerebro-spinal fluid, the application of brain spatulas, the movement of tissue, the swelling of brain structures, the resection of tissue, and a deformation following gravity. In consequence, the correlation of structures identified within the preoperative image data and within the actual situation of the patient becomes incorrect. As a result of this increasing misalignment, the precision of any neuronavigation setup deteriorates significantly during the ongoing course of the operation. Thereby, the location and the extent of structures are easily misinterpreted. This fact is of decisive relevance if the deep tumor margin is approached since it is normally reached at the end of a surgical procedure. At this time the inaccuracies reach their maximum which leads to the most dangerous situation of misinterpretation caused by the underlying neuronavigation system. This is the reason why a compensation for the brain shift including a correction of the neuronavigation system is essential. Consequently, the preoperative image data is completed by intraoperative scans in an increasing number of cases based on the availability of an appropriate imaging system within the operating room. This allows an update of the neuronavigation system according to the actual situation within the physical space of the patient.

Independent of the availability of intraoperative image data, various questions concerning the sources and effects of the brain shift and their correlation remain open. Furthermore, neurosurgical procedures are considerably improved if data of different modalities are simultaneously integrated within the neuronavigation system providing a more comprehensive representation of the situation. These data comprise information exclusively obtained preoperatively such as morphological data of angiographic procedures (Nakajima et al., 1997) or functional information resulting from magnetoencephalography (MEG) (Roberts et al., 1995, 1996, 1997), electroencephalography (EEG) (Chabrerie et al., 1997), functional MRI or positron emission tomography (PET) (Levivier et al., 1995, 2000). Considering the complexity of the underlying problem we suggest two different strategies. This accounts for a more ''practically oriented'' approach based on the neuronavigation system applied in clinical routine and a more ''theoretically oriented'' strategy analyzing the deformation with pre- and intraoperative MR data. The presented results demonstrate the value of both strategies contributing to a better understanding and a more quantitative evaluation of brain shift.

The paper is organized as follows. In Section 2 related work on the assessment of the brain shift phenomenon is discussed. Section 3 presents our own work showing a strategy applied in clinical routine. In Section 4 we introduce a model based approach using adaptively refined nonlinear voxel-based registration accelerated with OpenGL functions supported in graphics hardware. Finally, the results of our experiments with clinical cases are presented and discussed in Section 5.

2. Related work

In order to assess the magnitude of the brain shift there are primarily two different approaches: (1) direct measurements performed within the physical space of the patient, and (2) analysis of pre- and intraoperative image data based on registration procedures. Furthermore, experience is reported in literature (Audette et al., 1999) which is based on optically scanning the operation field in order to measure the difference of the pre- and intraoperative situation. However, there is a promising strategy evolving more recently which tries to simulate the brain shift based on an underlying mathematical model (Skrinjar and Duncan, 1999; Miga et al., 1999; Hata et al., 2000; Kyriacou et al., 2000; Ferrant et al., 2001; Skrinjar et al., 2002; Miga et al., 2000c; Miga et al., 2000a).

2.1. Direct measurement

The most intuitive and common approach to assess the brain shift is to use a pointer device within the applied navigation system. It allows one to measure distances between different structures directly within the surgical field. This is performed in the beginning of the operation and during tumor resection (Hill et al., 1997, 1998; Roberts et al., 1998; Dorward et al., 1998; Hartkens et al., 2003). The observed localization error is rated as the occurring brain shift. Compared to methods based on image data, these approaches are restricted to selective points and accessible structures of the surgical field. As a further drawback they are limited by the precision of the navigation system.

2.2. Intraoperative imaging

If intraoperative imaging is envisaged, there are basically three modalities available: X-ray CT, 3D ultrasound (US) and MRI. Using CT for neurosurgical application (Lunsford et al., 1984) the disadvantages are so far predominant. This is mainly related to the low soft tissue contrast and harmful nature of the required X-ray dose. By comparison, intraoperative US is gaining increasing importance (Comeau et al., 2000; Arbel et al., 2001). The additional overlay with MR or CT images leads to a considerably easier interpretation of the US images (Gobbi et al., 2000). Additionally, there are attempts to use these images to update the navigation system by deforming preoperative image data (Bucholz et al., 1997; Jödicke et al., 1998; Comeau et al., 2000; King et al., 2000). Major difficulties with this approach are mainly related to the different resolution of structures. However, compared to other modalities, intraoperative MRI seems to provide the most comprehensive potential to analyze deformations of brain structures. This is mainly related to its high contrast in soft tissue and the ability to adjust and optimize the imaging parameters according to different medical problems. As an important result, intraoperative MRI allows to evaluate the size of the intended resection in a comprehensive way (Black et al., 1997; Tronnier et al., 1997; Knauth et al., 1998; Hill et al., 1999; Ferrant et al., 2002). The resulting images give a global insight into the occurring shift and important target structures due to the detailed representation of soft tissue. In consequence, the modality makes it optimally possible to compensate for the decreasing precision of neuronavigation systems if the intraoperative image data is used for a correction of the system (Wirtz et al., 1997; Fahlbusch et al., 1998; Samset, 1999; Nabavi et al., 1999; Nimsky et al., 2001a). Multiple intraoperative acquisitions allow describing the direction and magnitude of intraoperative deformations in a comprehensive way (Nabavi et al., 2001). Furthermore, applying high-field (1.5 Tesla) MR scanners intraoperatively an improved image quality is achieved and advanced imaging techniques are performed (Maurer et al., 1998; Sutherland et al., 1999; Hall et al., 2000).

2.3. Mathematical models

Apart from compensating for the brain shift with intraoperative imaging, approaches based on different mathematical models have been developed. An important prerequisite of this strategy is data containing general information about the quantitative dimension of the brain shift. A variety of approaches (Skrinjar and Duncan, 1999; Hagemann et al., 1999b; Skrinjar et al., 2002) aim at predicting the occurring deformation in order to correct preoperative images. As a drawback, changes and effects caused by surgery are not taken into account. Other approaches follow a registration strategy to analyze the occurring deformation pursuing preoperative planning (Kyriacou and Davatzikos, 1998) and intraoperatrive brain deformation compensation (Ferrant et al., 2000; Audette et al., 1999). Optionally, these approaches are used to collect information allowing one to predict the brain shift. In this context, a more general and physically motivated approach relies on deformations of linear elastic or hyper elastic material of viscous fluids (Wollny and Kruggel, 2002; D'Agostino et al., 2002; Lester et al., 1998; Bro-Nielsen and Cotin, 1996; Christensen et al., 1996). Since all structures are treated as fluids, the specific physical behavior of individual parts is not taken into account. Complementary, a more complex approach (Hagemann et al., 2000, 2002) couples different physical models, simulating rigid, elastic, and fluid regions by using an appropriate physical description for each material. The necessary parameters of the underlying biomechanical model are based on an extensive literature study (Hagemann et al., 1999a). The resulting differential equations are solved with a finite element (FE) technique which results in a linear matrix system for each region. Adjacent systems are coupled through their common boundary. Another simulation approach based on a 3D FE model (Paulsen et al., 1999; Miga et al., 1999) applies parameters of the involved tissues which were experimentally obtained from animals (Miga et al., 2000a,b,c). In order to constrain the model, sparse surface information (Skrinjar and Duncan, 1999; Roberts et al., 1999; Skrinjar et al., 2002) is intraoperatively taken from different sources. So far, a 70% recovery of shifting structures is reported (Miga et al., 2000d) which still requires verification with human data on a larger scale. Alternatively, cortical constraints based on cortical sulci are used as sparse similarity information for nonrigid registration (Hellier and Barillot, 2003). In order to accelerate the complex calculation of the alignment transformation a shared-memory multiprocessor environment was applied (Rohlfing, 2003) or a cluster of PCs (Ourselin et al., 2002).

A drawback of most of the above mentioned approaches are the rather time consuming strategies which often result in high computational costs of several hours. They mainly rely on preoperative images and possibly some sparse intraoperative data. Another group of contributions deals with nonlinear registration of pre- and intraoperative MR data. In this context other groups have already reported on the assessment of brain shift with intraoperative MRI (Maurer et al., 1998; Hill et al., 1999). They presented nonlinear registration strategies to calculate the occurring deformation offline. They use free-form deformation based on B-splines using normalized mutual information (Schnabel et al.,

2001; Rohlfing et al., 2003; Schnabel et al., 2003) and an optical flow method (Hata et al., 2000). Furthermore, the volumetric deformation is calculated using a linear elastic biomechanical FE model based on initial surface tracking (Ferrant et al., 2001).

3. Imaging approach

3.1. Neuronavigation

Since December 1995 the Department of Neurosurgery of the University of Erlangen-Nuremberg has been equipped with a "twin operating theater" consisting of two neighboring operating rooms (Fahlbusch et al., 1998; Steinmeier et al., 1998). In the radio frequency-shielded part an open MR scanner (0.2 Tesla Magnetom Open, Siemens AG, Erlangen, Germany) and all MR compatible equipment required for neurosurgery has been installed including a system for anesthesia. The second room is a conventional operating theater containing a modern neuronavigation system (MKM, Zeiss, Oberkochen, Germany) which is not MR compatible.

If necessary, the patient is intraoperatively moved from the conventional operating theater into the MR scanner using an air-cushioned OR table. Thereby, the extent of the resection of a tumor can be evaluated. If surgery is continued, the preoperative MR dataset is replaced and the neuronavigation system is corrected based on the intraoperative MR images.

Intraoperative imaging has been applied in 330 patients in the last five years. Among the group of glioma patients ($n = 106$) in 63% remaining tumor was assessed which was successfully removed during further surgery after localization in 26%. Thereby, the rate of gross tumor removal was increased especially in the low-grade tumors. In a subset of 32 glioma patients the magnitude of the brain shift was evaluated. All glioma patients undergoing intraoperative imaging were among the more difficult cases with lesions located near eloquent brain areas. As can be seen in Table 1, a consecutive correction of the neuronavigation system was performed in eight glioma patients (Nimsky et al., 2000, 2001b).

In addition to anatomical data, the neuronavigation strategy was also supported by functional information in over 120 patients. Based on respective measurements with MEG and functional MRI the location of the motor cortex and the speech area is labeled within the preoperative anatomical MR data. Due to the intraoperative visualization of the combined anatomical and functional image data a fast and precise identification of eloquent brain area is achieved. In consequence, a more complete resection and a reduced morbidity are achieved in case of tumors located in the closer vicinity or within eloquent areas (Ganslandt et al., 1997, 1999; Nimsky et al., 1999, 2003).

3.2. Registration and visualization

In order to evaluate the extent of the tumor resection and the amount of brain shift, a registration of the pre- and intraoperative MR data is performed with the neuronavigation system. Having acquired intraoperative MR data a rigid registration with the preoperative images is performed using the STP 4.0 software (Zeiss, Oberkochen, Germany). It requires 6–12 landmarks which are either anatomical or fiducial in order to calculate the initial rigid registration and to evaluate the alignment quality based on the root mean square error. The quality of the registration was visually evaluated by inspecting the alignment of the skin surface equally delineated within the pre- and the intraoperative image data. As an additional information the location of the basilar artery is assessed since it is supposed to be only slightly influenced by the brain shift.

For the consecutive analysis of the brain shift a 2D strategy is applied for the visualization of the registration result. It provides a split screen representation showing the pre- and the intraoperative data separately within communicating windows including a linked cursor. Additionally, for a more intuitive overlay of the registered images one dataset is presented within a magic lens (Bier et al., 1997; Viega et al., 1996), which is moved or resized interactively within a window containing the other dataset in the background. Using alpha-blending (Porter and Duff, 1984) corresponding slices are optionally overlaid. For the purpose of documentation the maximum displacement of the following structures were measured: cortical surface, deep tumor margin, anatomical midline, and ventricular system. In all cases the direction of this displacement was considered by assigning positive values for a movement towards the surface and negative values for a movement from the surface. Except for the ventricular system where the average displacement of at least six landmarks was taken as absolute value.

4. Registration approach

In addition to the presented imaging approach, a model based strategy is suggested which focuses on efficiently compensating for brain shift using pre- and intraoperative MR data. It is required for a further step in order to consider image data such as functional information from fMRI or MEG which is only preoperatively available. For this purpose nonlinear voxel-based registration based on mutual information has been applied. The huge number of interpolation operations is one of the most limiting factors for the performance of voxel-based registration. In consequence, this fact is often responsible for high computation times prohibiting intraoperative application. We improve speed con-

siderably using piecewise linear transformations and OpenGL functions supported in graphics hardware. This approach is built on top of our previous work (Hastreiter and Ertl, 1998) which introduced hardware accelerated 3D texture mapping for rigid registration. It represents an extension to pure software based approaches (Wells et al., 1995; Collignon et al., 1995; Studholme et al., 1996, 1999). Contrary to initial results presented in (Hastreiter et al., 2000), the approach became more robust using pre-segmented brain volumes. Additionally, the efficiency was further improved by the use of adaptive refinement of the underlying control point grid.

4.1. Similarity metric

Voxel-based registration takes into account the entire grey value information of the image data and does not require an explicit segmentation. The choice of an appropriate similarity metric is important for the evaluation of the quality of registration during the optimization of the underlying transformation. For both mono- and multimodal image data mutual information, as initially suggested in (Wells et al., 1995; Collignon et al., 1995), has proven to be more robust compared to other registration techniques (West et al., 1999).

Considering a floating dataset F and a reference dataset R, the registration procedure evaluates the data values of both volumes at corresponding locations. The marginal probability distributions of the sample values from F and R are denoted by $p_F(f)$ and $p_R(r)$, respectively. Having applied the registration transformation T, the floating dataset F is interpolated based on the grid of R resulting in the joint probability distribution $p_{RF}(r(x), f(T(x)))$. For convenience, r and $f(T)$ are used instead of $r(x)$ and $f(T(x))$.

If both datasets, and $f(T)$ are identical, the joint probability distribution amounts to

$$p_{RF}(r, f(T)) = p_R(r) = p_F(f(T)). \tag{1}$$

In the other case, the joint probability distribution satisfies

$$p_{RF}(r, f(T)) = p_R(r) \cdot p_F(f(T)), \tag{2}$$

if both signals are statistically independent. Considering both marginal cases mutual information is defined as

$$I_{RF} = \sum_{(r, f(T))} p_{RF}(r, f(T)) \log\left(\frac{p_{RF}(r, f(T))}{p_R(r) \cdot p_F(f(T))}\right), \tag{3}$$

summing over all pairs of samples $(r, f(T))$ at corresponding locations. Consequently, the registration solution is reached if the parameters of T are optimized in such a way that mutual information reaches a maximum, e.g.,

$$I(r, f(T_{\text{opt}})) = \max_T [I(r, f(T))]. \tag{4}$$

For the optimization of Eq. (4) an appropriate numerical algorithm for multidimensional minimization is required. Direction set methods are frequently used if the explicit evaluation of partial derivatives must be avoided. There are numerous strategies which mainly differ in the set of direction vectors they use. In the suggested approach Powell's algorithm was chosen, which generates a set of mutually conjugate direction vectors for the iterations (Press et al., 1988).

4.2. Piecewise linear transformation

A drawback of voxel-based methods are the high computational costs, which are dominated by the interpolation of the volume data. Therefore, acceleration techniques are of great importance. Furthermore, a compensation for brain shift requires to use nonlinear transformations in order to model local deformations of the brain.

Aiming at clinical application, the idea is to leverage the texturing capabilities of modern graphics hardware for accelerated interpolation. Experiments with piecewise curved transformations as well as polynomial and Bézier tensor product patches turned out to be extremely time-consuming. Implementations were restricted by the high complexity of polynomial patches and by limited hardware support for Bézier splines. Alternatively, we applied piecewise linear transformations (Rezk-Salama et al., 2001) to approximate nonlinear deformations.

The mathematical model of the volumetric deformation is based on a subdivision of an object into a set of sub-cubes as displayed in Fig. 1. Representing the volumetric object as 3D texture, the deformation is modeled by shifting the texture coordinates at the free vertices. It is propagated into the interior of a patch by trilinear interpolation.

Initially, the floating dataset is uniformly subdivided into a fixed number of linear patches. Since deformations are restricted to central regions of tomographic data, the positions of the vertices at the boundaries remain fixed. All inner vertices are transformed during the optimization of the similarity metric according to the best alignment with the reference dataset. By slicing the described deformation model into planar polygons, similar to texture based volume rendering (Cabral et al., 1994), the optimization process is accelerated significantly. The efficiency of the presented approach can be further enhanced since only a subset of the volume needs to be corrected for clinical application. This was achieved by reducing the necessary number of free parameters with an adaptive subdivision scheme.

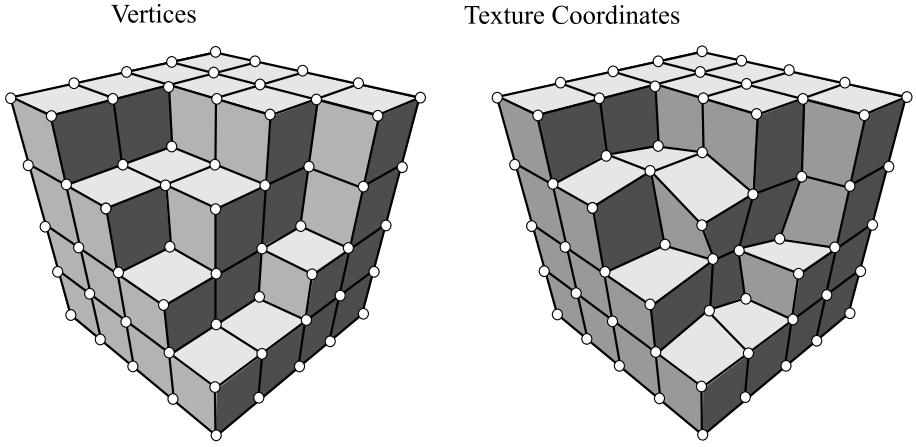

Fig. 1. Uniform subdivision of a volume into piecewise linear patches to approximate nonlinear transformations. Some patches have been removed to reveal the interior.

4.3. Adaptive subdivision

A good approximation of the nonlinear transformation using uniform subdivision leads to a large number of piecewise linear patches. In order to reduce the amount of free vertices for optimization, an adaptive refinement scheme was used to produce a hierarchical octree structure.

Starting with an initial decomposition of the volume data, the contribution of each patch to mutual information is calculated. Based on a criterion for local refinement further vertices are introduced for each patch. This results in an adaptively refined octree structure, as demonstrated in Fig. 2(a). At the boundary between patches with different refinement levels, constrained vertices are required. Otherwise, gaps occur in texture space, as shown in Fig. 2(b). Contrary to the fixed vertices, the location of the constrained vertices depends on the position of the free neighboring vertices.

Note that the decomposition of the volume into an octree hierarchy is performed only once at the beginning of the registration. Thereby, the total registration time is effectively limited. Two different examples in Fig. 3 illustrate the initial refinement. During the iterations of the consecutive registration process the locations of the free vertices are optimized and the positions of the constrained vertices are updated accordingly. This process is iteratively repeated until the requested accuracy is reached.

In order to decide about the subdivision of patches, a refinement criterion is used. Defining mutual information in terms of entropy, there is an upper limit (Maes et al., 1997) according to

$$I_{RF} \leqslant \min(H(R), H(F)), \tag{5}$$

with $H(R)$ and $H(F)$ representing the entropy of the random variables R and F amounting to

$$H(R) = -\sum_{x} p_R(r) \log(p_R(r)) \tag{6}$$

and

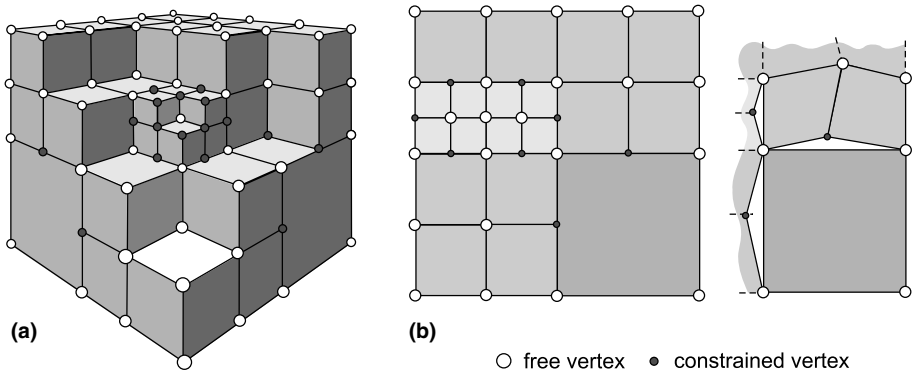

Fig. 2. Adaptive subdivision generates a hierarchical octree structure of piecewise linear patches and significantly reduces the number of free vertices for the optimization procedure (a). Constrained vertices are required on edges or faces between patches of different subdivision levels. Ignoring such constraints would lead to gaps in texture space (b).

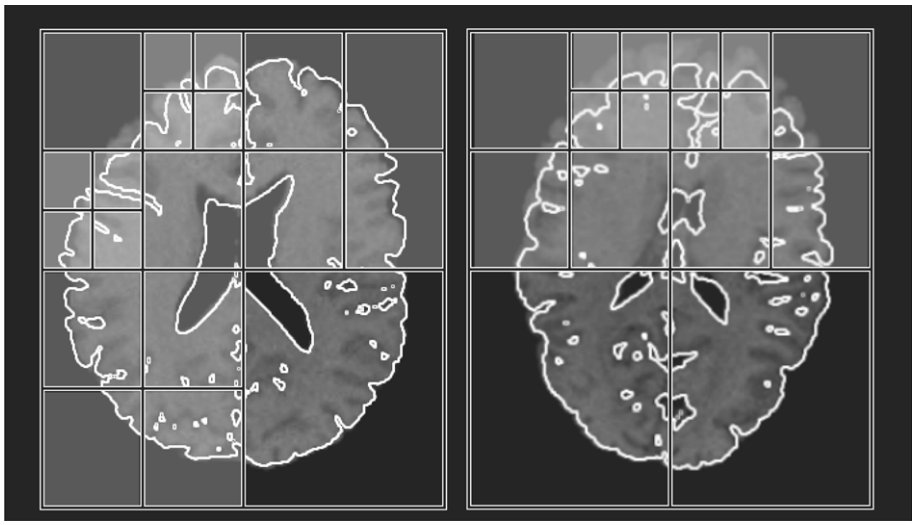

Fig. 3. Depending on the location of the occurring deformation two different subdivision schemes are presented.

$$H(F) = -\sum_{x} p_F(f)\log(p_F(f)). \tag{7}$$

For every linear patch g_i both the contribution

$$I_i = \sum_{(r,f(T))\in g_i} p_{R_iF_i}(r,f(T))\log\left(\frac{p_{R_iF_i}(r,f(T)}{p_{R_i}(r)\cdot p_{F_i}(f(T))}\right), \tag{8}$$

to the overall mutual information $I_{R,F} = \sum_i I_i$ and, according to Eq. (5), the upper limit

$$H_{\min}(R_i,F_i) = \min(H(R_i),H(F_i)), \tag{9}$$

are computed, respectively. This results in

$$0.0 \leqslant \frac{I_i(R,F)}{H_{\min}(R_i,F_i)} \leqslant \vartheta \leqslant 1.0, \tag{10}$$

which means that a patch is subdivided if the ratio $I_i(R,F)/H_{\min}(R_i,F_i)$ is smaller than a user-defined threshold ϑ. This threshold ϑ is heuristically set to 0.7–0.8. Taking into account the upper limit of mutual information according to Eq. (5) the ratio represents a maximum for perfect registration if the ratio equals to 1. Since this situation is never reached in reality, this threshold ϑ is heuristically set to 0.7–0.8 which is close enough to the optimum.

Note that in case of very small patches, the evaluation of this refinement criterion becomes less accurate. This is caused by the limited number of samples available for the calculation. However, this problem is efficiently circumvented using hardware accelerated interpolation as described subsequently. This allows increasing the sampling rate conveniently.

The probability distributions are based on the calculation of the respective 1D and 2D histograms. In order to reduce the computational effort for the evaluation of the histograms, the image data was initially scaled to 256 grey values. According to our experience, this proved to be sufficient to ensure a robust registration.

4.4. Hardware acceleration

The subsystem of high-end workstations and an increasing number of PC graphics cards provide 3D texture mapping capabilities allowing hardware accelerated trilinear interpolation. Based on the experience with direct volume rendering, the interpolation of the floating dataset is considerably assisted as presented in (Hastreiter and Ertl, 1998) for rigid transformations. A comparable strategy was applied for the suggested piecewise linear transformations.

Having loaded the floating dataset into 3D texture memory, slice images are reconstructed, each of them corresponding to a slice of the reference dataset. In order to model the patches of the piecewise linear transformation, every slice defined for the floating dataset must be triangulated explicitly.

In order to accurately propagate the deformation to interior parts of the patches, trilinear interpolation of the texture coordinates given at the vertices of the slice polygons must be performed. An explicit triangulation of the nonplanar quadrilaterals in texture space is essential, as illustrated in Fig. 4. In column a the desired trilinear interpolation is displayed. The automatic tessellation which is internally performed by the graphics hardware will lead to a bad approximation of the trilinear deformation since the grey triangle (see column b) is not affected by the deformation. As a solution to this problem, inserting an additional vertex in the middle of the polygon results in a sufficiently close approximation of the original trilinear deformation (compare column c). This also provides a correct triangulation of the nonplanar texture map which results from the deformation in 3D texture space.

In order to perform trilinear interpolation of the floating dataset, the polygons defined by all vertices

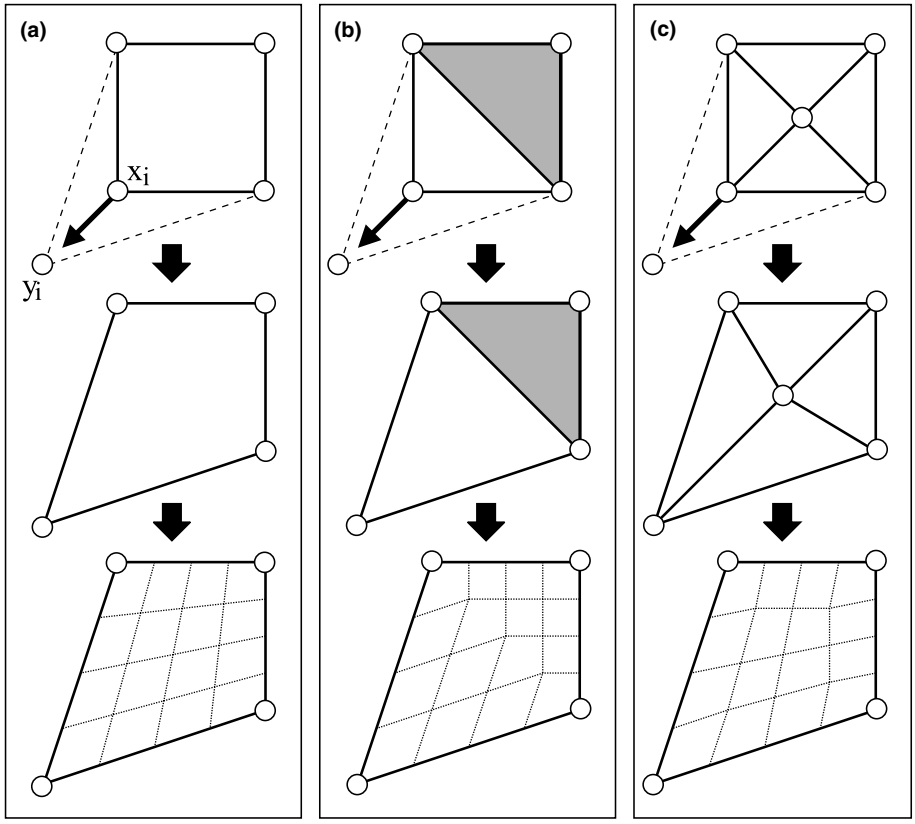

Fig. 4. Contrary to the desired trilinear interpolation (a), internal tesselation within the graphics hardware (b) results in a very bad approximation with linear interpolation in barycentric coordinates. Inserting an additional vertex (c) leads to four triangles with barycentric interpolation providing sufficient approximation of trilinear interpolation.

after triangulation in physical space are projected onto the image plane by drawing them into the frame buffer. Simultaneously, the locations of the vertices are also used as 3D texture coordinates which are adjusted according to the registration transformation. Thereby, the location of the free vertices is changed in texture space leading to a deformation of the volume. During rasterization the polygons drawn into the frame buffer are textured with their corresponding image information obtained by trilinear interpolation directly performed with 3D texture mapping. Thereafter, the contents of the frame buffer is read out in order to compute mutual information. This procedure is repeated for all slices of the reference data and every iteration step of the optimization procedure.

5. Results and discussion

5.1. Imaging approach

For the pre- and intraoperative MR data a T1 weighted 3D-FLASH (fast low angle shot) gradient echo sequence was applied. In all cases the obtained volumes consisted of images with a matrix of 256^2 pixels and 112 slices. The size of the voxels was set to $0.9 \times 0.9 \times 1.3$ mm^3. If the tumor was enhanced within the preoperative images, an additional contrast agent (20 ml Gadolinium-DTPA) was applied intraoperatively. In case of gliomas the intraoperative imaging also included a T2 weighted inversion recovery scan. Thereby, in addition to an optimized detection of tumor remnants, further information was obtained about possible leakage of contrast agent at the resection border or a diffuse spreading of contrast enhancement related to surgical manipulations.

Note, the intraoperative MR images are darker and poorer in contrast compared to the preoperative images, although the same pulse sequence was used for both data. This effect is related to a special coil for intraoperative application and artifacts caused by the operating environment.

The evaluation of the brain shift performed with point based rigid registration of pre- and intraoperative MR images confirmed the clinical experience in case of glioma patients. The occurring deformation is influenced by the different parameters of the tumor (type, size, localization), the position of the patient, the size of craniotomy and the opening of the ventricular system. The measurements revealed a maximal shift of the cortex surface of up to -17.4 mm while the anatomical midline was displaced in the range of 2.3 to -4.0 mm.

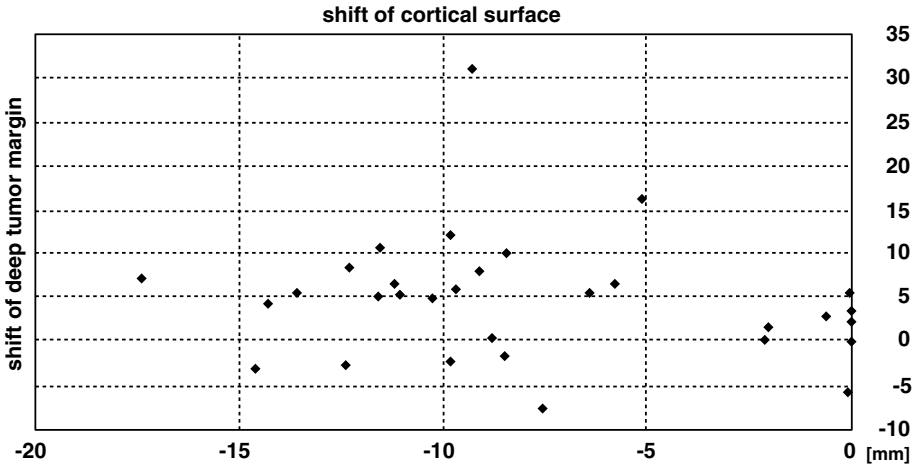

Fig. 5. Shift of the cortical surface versus the deep tumor margin occurring during surgery in 32 glioma cases. The amount of deformation is clearly uncorrelated in each case demonstrating the independent behavior of both structures.

Simultaneously, the deep tumor margin was shifted in the range of −7.9 to 30.9 mm. These results confirm the general necessity to correct the brain shift intraoperatively in order to reliably use a neuronavigation system. To demonstrate the complexity of the deformation phenomenon, Fig. 5 shows the amount of shift determined for the cortical surface and the deep tumor margin in 32 glioma cases. As can be seen from the diagram, the measurements of both structures are uncorrelated revealing their independence. In all cases the intraoperative acquisition was carried out when the neurosurgeon had the impression that the tumor was either completely resected or infiltration of eloquent brain areas prohibited further resection.

The neuronavigation system is effectively updated and corrected with intraoperative images which allow considering brain deformations and surgery related changes. For this purpose MRI is an optimal imaging technique providing comprehensive visual control of the resection. This is of major interest in case of gliomas in order to achieve a more complete resection (Steinmeier et al., 1998). However, this strategy requires further support by mathematical models to gain an improved understanding of all related effects. Evolving results contribute to simulate brain deformations, which might finally allow a reduction of intraoperative imaging.

5.2. Registration approach

The same pre- and intraoperative MR datasets were used for the evaluation of the adaptive nonlinear registration approach (see Table 1). Fig. 6 illustrates the obtained results for a patient with a large left-sided fronto-temporal low-grade astrocytoma. The intraoperative images were acquired after partial tumor removal. In comparison to the original pre- and intraoperative data, a selected pair of slice images shows the compensation for brain shift after nonlinear alignment. In this example the deformation amounted up to 25 mm.

In Fig. 9 a further example is presented which shows the results of the applied nonlinear alignment in comparison to a rigid registration. The overlay images clearly demonstrate how the occurring deformation was effectively compensated for with the applied nonlinear strategy. Thereby, the extent of brain shift was analyzed at the borders and especially at inner areas which are crucial for surgery. Subtraction images are shown to visualize the quality of the obtained alignment.

For the quantitative evaluation of the presented registration approach anatomical points were defined in the pre- and intraoperative data of each patient. Eight of these points which could be securely identified were chosen around the ventricular system in each dataset. Further landmarks were selected on an individual basis at the cortex depending on the maximal shift of brain surface. Finally, points describing the deep tumor margin were defined in order to evaluate the quality of alignment in the area of resection. Having applied the resulting registration transformation, the distances between corresponding points in the intraoperative and the respectively aligned preoperative volumes were calculated. The resulting values are summarized in Table 5 for rigid transformations and in Table 6 for the suggested strategy with piecewise linear transformations using level three for the refinement. The analysis and a comparison of both tables clearly demonstrates the accuracy of the presented nonlinear approach and the improvement compared to the initial rigid registration. Particularly, the shift in the area of resection was reduced to a minimum. Notably a distance of about 6–8 mm for the datasets 2 and 8 and an even higher distance of up to 20 mm for the datasets 5 and 6 was compensated with a remaining difference of about 1.5–2.0 mm. This, however, is close to the voxel size in z-direction.

Table 1
An update of the neuronavigation system was performed in case of eight glioma patients

Age, gender	Location WHO grade diagnosis	Functional imaging	MRE (mm)
8, m	rt. parietal, II oligodendroglioma	–	0.39
68, m	rt. precentral, IV glioblastoma	MEG	0.79
31, f	lt. precentral, IV glioblastoma	MEG, fMRI	1.5
27, m	lt. frontal, I astrocytoma	–	0.8
45, m	lt. precentral astrocytoma	MEG	2.3
37, m	rt. precentral astrocytoma	MEG	2.0
32, m	lt. frontal, IV glioblastoma	–	0.77
26, m	lt. frontal, IV oligoastrocytoma	MEG	2.1

The following is addressed: age [years], gender [f: female, m: male], tumor location [left (lt), right (rt)], histopathological diagnosis including the WHO (world health organization) grade, the applied functional imaging modalities, and the mean registration error (MRE) of the intraoperative update related to fiducial markers attached to the patient.

Comparably good results were also achieved for the points defined at the cortex and at the lateral ventricles. Some exceptions are found in datasets 1, 4 and 5 with remaining differences exceeding 2.5 mm. Additionally, the overall gain achieved with nonlinear compensation is expressed with statistical measures calculated over all the distances of each patient. The general reduction of the root mean squared errors (RMS) and the variances further emphasize the value of our work.

An essential part of the presented approach is the subdivision of the control point grid. For an overview, Table 2 summarizes details about the different levels in case of uniform refinement. Adaptive subdivision significantly reduces the total number of free grid points, thus speeding up the optimization procedure. For the example in Fig. 9 about half of the maximal number of vertices in level three was used. As a further advantage of this strategy the registration efforts are focused on the regions of major deformation. Thereby, better alignment quality is achieved for shifted parts of the brain (e.g. at the cortex or in the resection area) whereas other parts are treated with a coarser grid and consequently less accuracy. In order to limit the effort of this refinement procedure the brain volume is segmented initially. For this purpose an automatic volume growing procedure is used which is additionally restricted with user-defined bounding boxes. Finally, segmentation errors were corrected with manual labeling. In all cases the required processing time for this step was in the range of 10–15 min and lead to sufficiently separated subvolumes representing the brain surface. As a result, the applied pre-segmentation circumvents the problematic transition from flexible brain tissue to surrounding regions of the head that are not important for the investigation of brain shift.

The stated threshold in Eq. (10) was chosen in order to control the subdivision. In this context, the hierarchical octree structure of the control point grid is generated automatically evaluating the similarity of corresponding patches. Using smaller thresholds than the suggested range of values causes the adaptive partitioning to work with reduced sensitivity which deteriorates the quality of alignment and the timing of the optimization procedure. In the presence of acquisition noise, the quality of the presented approach is not directly influenced which is mainly related to the robustness of the registration measure. However, if there is a disproportionally high amount of noise some filtering should be applied in the beginning. This ensures a meaningful calculation of mutual information in individual patches.

An adequate modeling of the nonlinear deformation function requires a high level of adaptive subdivision using piecewise linear patches due to the rigid structures surrounding the deformed brain. As a drawback, the suggested approach is so far limited by a certain level of subdivision without increasing the resolution of the images and the related computational costs. Therefore, the brain volumes were segmented in the pre- and intraoperative MR datasets after rigid registration. Optionally, the nonlinearly aligned brain volumes were finally fused again with the remaining structures (see Fig. 7). As a result of this strategy, the performance and the robustness of the registration process was increased.

Throughout our study a Silicon Graphics Onyx2 (R10000, 195 MHz) with BaseReality graphics hardware was used. As an initial experiment, 2D registration was performed with images consisting of 256×256 pixels in order to compare software and hardware based approaches. Table 3 shows that hardware accelerated

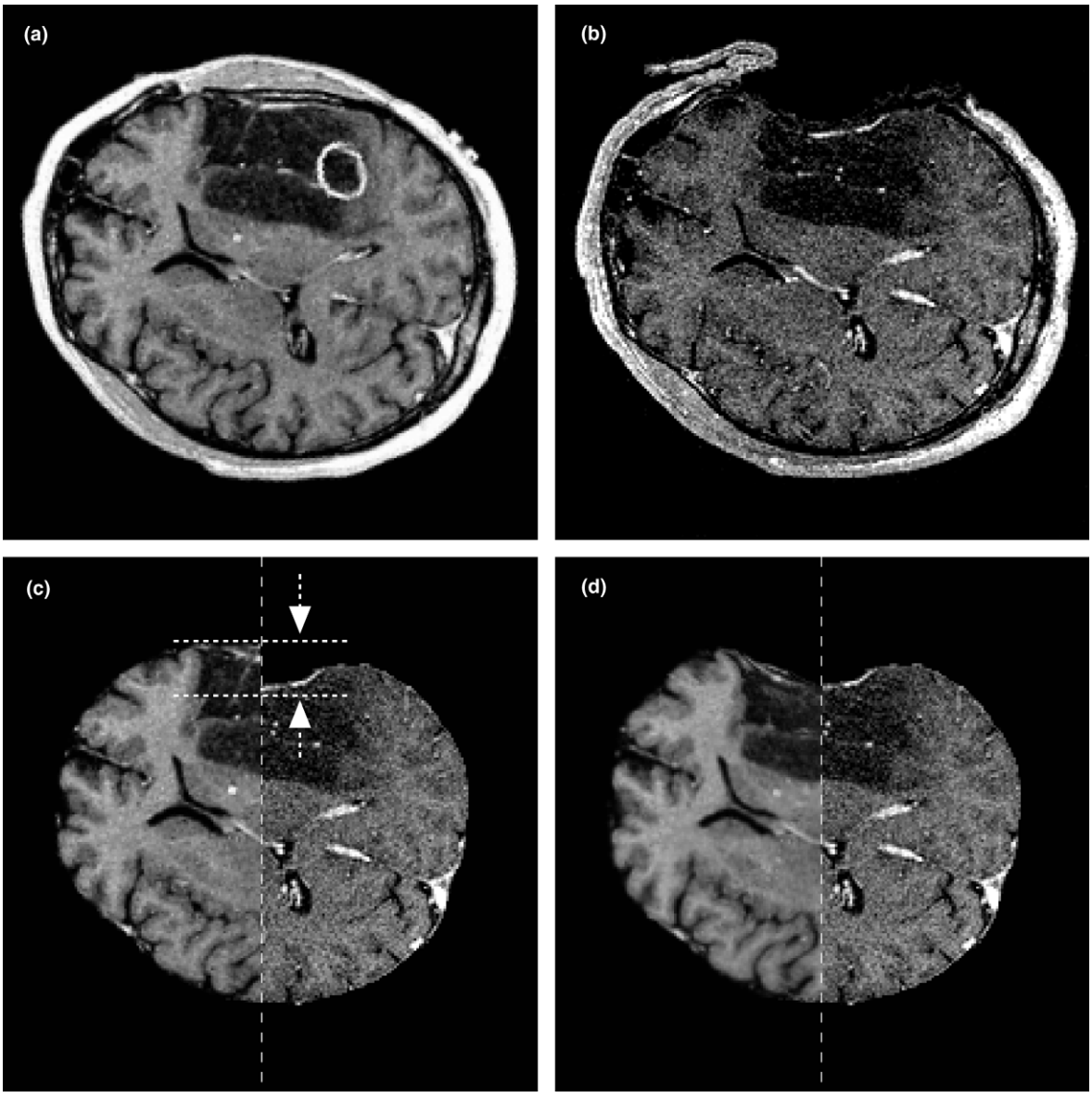

Fig. 6. Registration of pre- (a) and intraoperative (b) MR data. Functional data for the localization of speech-relevant areas localized with magnetoencephalography are integrated in the preoperative data (white circle). The comparison of the undeformed data (c) (left side pre-, right side intraoperative) and the registration result (d) demonstrates the compensation for brain shift (dotted lines in c serve for the easier orientation to see the extent of brain shift at the cortical surface).

Table 2
Overview of the subdivision scheme showing the applied levels of refinement, the grid spacing for the x/y and z direction and the maximum number of free grid points in case of uniform refinement

Refinement level	Cell size x,y (mm)	Cell size z (mm)	Grid points (number)
I	115.2	83.2	1
II	57.6	41.6	27
III	28.8	20.8	343

texture mapping is about two orders of magnitude faster than a software based technique. For these tests an initial 4×4 subdivision and a maximum refinement level III was applied. The comparison between hardware and software based registration was only performed for the 2D case. Due to the discouraging results of the 2D software approach in terms of computation time, the implementation of 3D software based registration has not been followed up.

The performance measurements for 3D registration are shown in Table 4. The results demonstrate the superiority of adaptive subdivision compared to a static uniform grid. Note that the adaptive approach has no negative influence on the accuracy. The chosen refinement criterion (see Eq. (10)) assures that only regions of insufficient registration are further

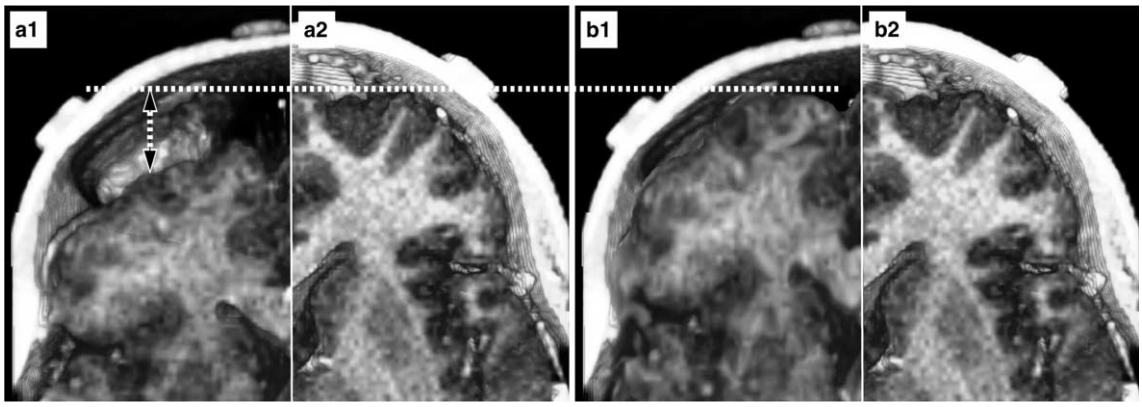

Fig. 7. Voxel-based registration of pre- (a2, b2) and intraoperative (a1, b1) MR data based on mutual information and graphics hardware for acceleration: (left) rigid transformation – (right) piecewise linear transformation (dotted line serves for better orientation).

Table 3
Performance of 2D registration using the software and hardware based strategy

Registration type	Image size (voxels)	Voxel size (mm)	Time (s)
2D software	256×256	0.9×0.9	1.1×10^3
2D hardware	256×256	0.9×0.9	22

Table 4
Performance of 3D registration for uniform and adaptive subdivision using hardware accelerated piecewise linear transformation with respect to the number of free vertices (#FV) and the resulting degrees of freedom (#DOF) for optimization for a data set of size 256^3

Registration type	#FV	#DOF	Time (s)
Uniform level II	27	81	≈60 min
Uniform level III	343	1029	≈24 h
Adaptive level III	16–20	48–60	≈20–30 min

subdivided. Thus, the results achieved with this strategy are not less accurate than the ones achieved by the uniform grid using a global threshold. In the first adaptive subdivision step the volume cube was decomposed into eight sub-cubes. In the typical case the subdivision criterion selects 4–6 of the resulting subcubes for further refinement. In the third step usually 10–20% of the patches from level II are further subdivided up to level III.

Interpolation capabilities of graphics hardware were extensively used, in order to improve the computation time of the presented approach. For this purpose the floating volume was loaded to graphics memory using the OpenGL command *glTexImage3D*. If a polygon is textured by assigning respective texture coordinates the texture filtering techniques of the underlying hardware are automatically accessed which supports trilinear interpolation. For the applied SGI Onyx2 a maximum of 200×10^6 trilinear interpolation operations per second is obtained which ensures high rendering performance. However, in order to evaluate the voxel-based similarity measure, the frame buffer contents must be read out and transferred into main memory using the comparably slow OpenGL command *glReadPixels*$(\cdots)$. This is in relation to the bus bandwidth between the host and the graphics subsystem which is the most limiting factor and does not allow a further improvement of the performance. One possible solution to this problem would be to also calculate the similarity measure directly within the graphics hardware. Although there are promising developments of forthcoming programmable graphics subsystems, the currently available hardware is still not flexible enough for complex computations such as mutual information.

A major concern of the presented work was the attempt to accelerate the huge number of interpolation operations required for voxel-based registration using graphics hardware. This approach was pursued to use the procedure during neurosurgery. Since the applied 3D texture mapping hardware supports linear interpolation only, certain limitations have to be faced in comparison to higher order strategies. As a certain drawback, the applied piecewise linear transformation does not include any smoothness constraint as it is naturally inherent in spline interpolation. However, from our experience, the magnitude of the deformation is small enough such that the lack of smoothness is hardly noticeable.

To evaluate the refinement criterion, the 2D histogram of a single patch must be computed. However, this strategy is limited by the number of sample points used for evaluating mutual information. On the other hand, the available information is bounded and inaccurate due to the discrete nature of the voxels. Using texture mapping hardware this situation is influenced in a way by zooming the respective polygons to a viewport of appropriate size, when drawing into the frame buffer. Thereby, the interpolation leads to a broader spectrum of intensity values which are of equal quality compared to the original values. This increased number of pixels

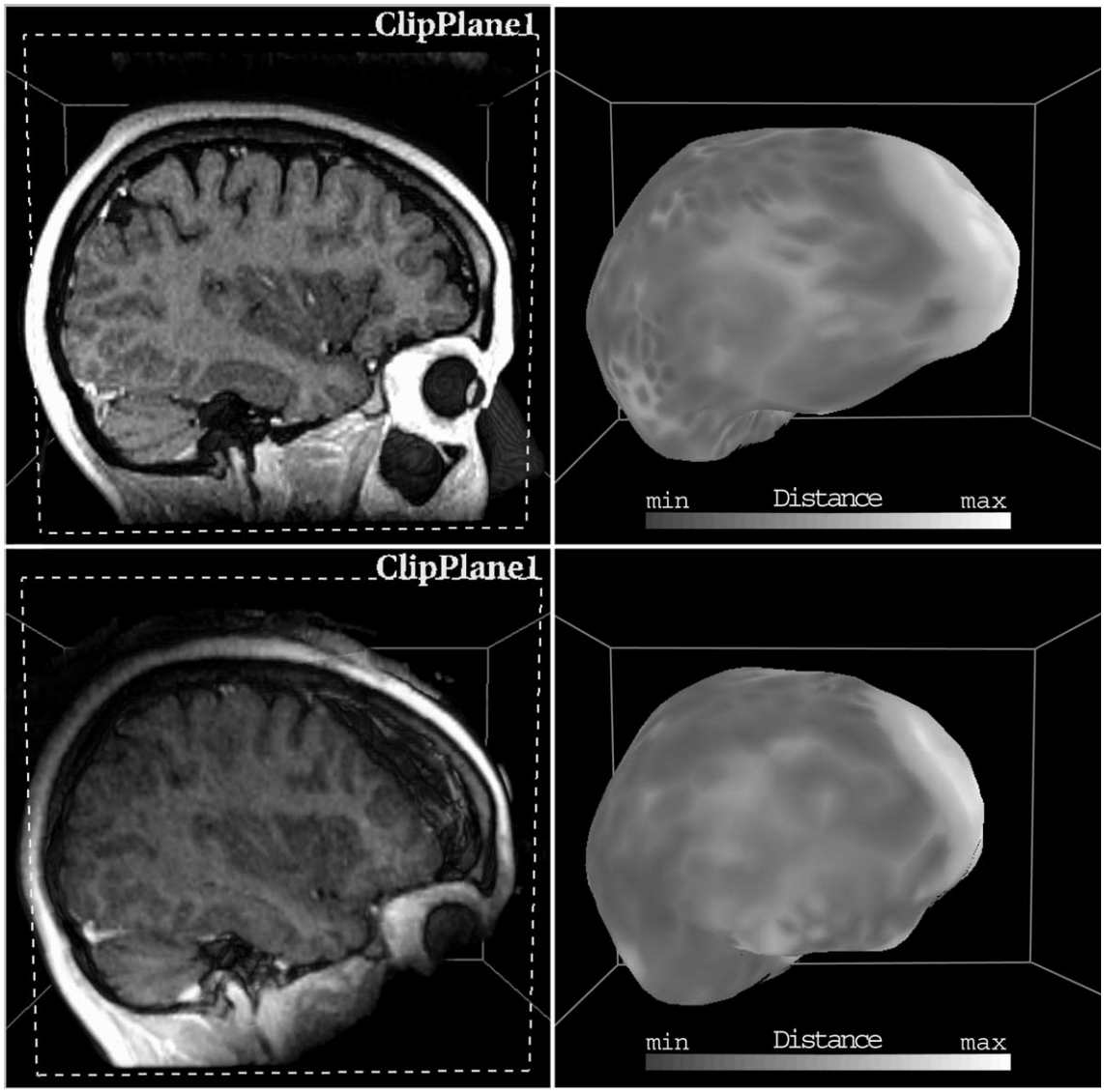

Fig. 8. Comparison of direct volume rendering (left) and grey scale encoded polygonal models (right) based on preoperative (top row) and intraoperative MR (bottom row) data showing brain shift. Direct volume rendering shows detailed anatomical information having applied a clip plane suppressing a half space from rendering. The polygonal models of the brain surface give a quick overview of the overall deformation. They were extracted after rigid registration of the volume data using an automatic voxel-based approach based on mutual information.

leads to a smoother and improved computation of mutual information with little loss in performance.

5.3. Visualization

In order to evaluate the registration results (see Fig. 10), the MR data was visually analyzed with a 2D approach on a slice by slice basis. Alternatively, a 3D approach (Hastreiter et al., 1998; Tomandl et al., 2001; Rezk-Salama et al., 2000) based on direct volume rendering was used leading to an improved visualization since it considers the spatial nature of the image data.

For a more comprehensive analysis of brain shift, polygonal surfaces of the the pre- and intraoperative brain surface were additionally extracted according to an approach suggested in (Lürig et al., 1998; Hastreiter et al., 2000). As demonstrated in Fig. 8, the consecutive visualization permits a global understanding of the occurring cortex deformation. Optionally, information about the surface distances was mapped onto the models using color coding. Thereby, a quick overview about the localization and extent of the brain shift was given which is considered to be helpful for clinical application. As a certain drawback of this strategy, the distance between initial and deformed surfaces can underestimate the actual displacement if within-surface correspondences (homologies) are not taken into account. In consequence, registered surface regions of the cortex might not be functionally or anatomically the same and a greater displacement could occur than the distance metric implies.

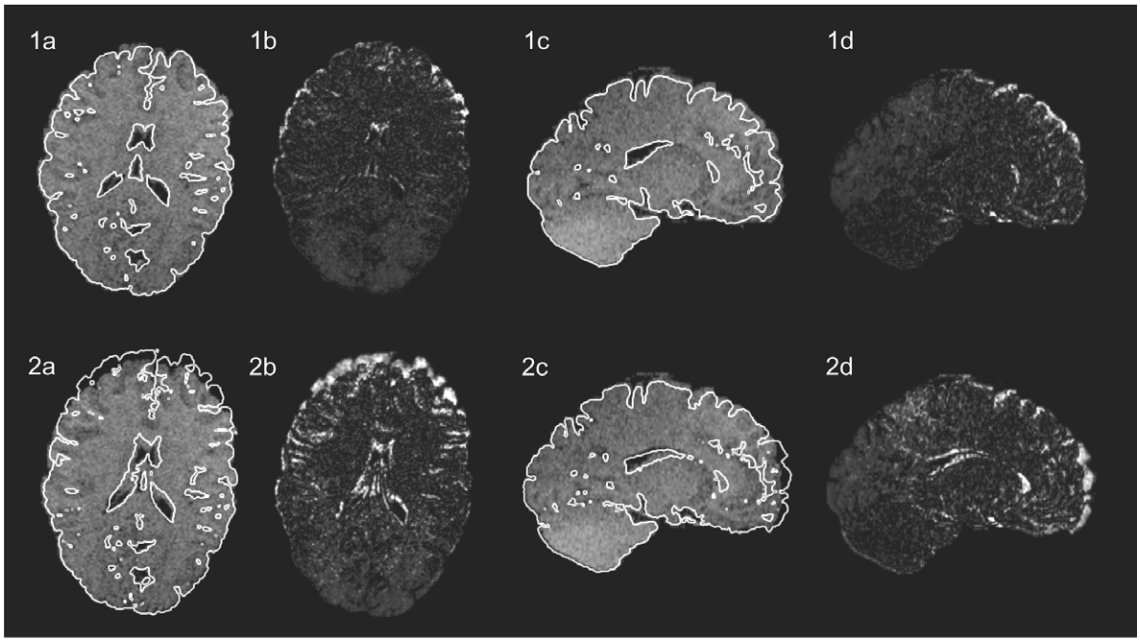

Fig. 9. Comparison of the results after voxel-based nonlinear (upper row) and rigid (lower row) registration. Contours extracted from the preoperative data are overlayed onto the intraoperative images for axial (1a, 2a) and saggital (1c, 2c) slices. Additionally, subtraction images (column b, d) demonstrate the absolute value of the grey value differences.

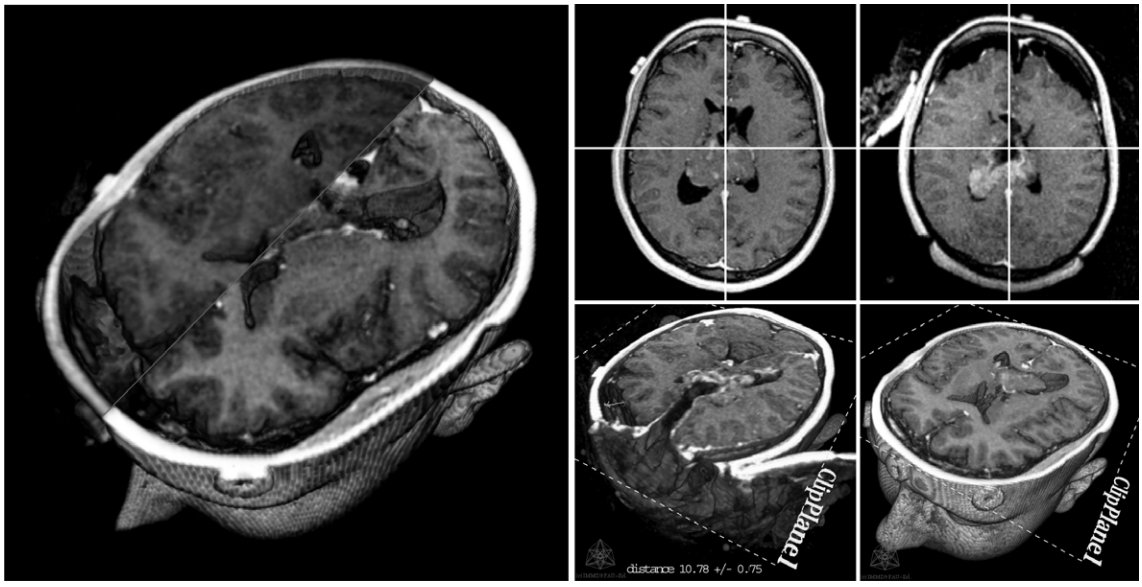

Fig. 10. Comparison of pre- and intraoperative MR datasets after rigid registration. Taking into account the spatial nature of the MR data the standard 2D visualization is supported by a 3D approach using direct volume rendering.

6. Conclusions

Due to the intraoperative deformation of the brain referred to as brain shift, the reliability of neuronavigation based on preoperative images deteriorates with time following the craniotomy. The presented work contributes to a better understanding of the sources and effects of this phenomenon using pre- and intraoperative MR data. In addition to updating the neuronavigation system based on the provided images, mathematical models are important for a more comprehensive analysis. Using OpenGL functions supported in graphics hardware and adaptive refinement of the control point grid, a successful attempt has been made to improve the speed of alignment, thus making it suitable for intraoperative use. Although the obtained results are prom-

Table 5
Quality of rigid registration evaluated with distances [mm] of corresponding points P_i defined in the rigidly transformed preoperative and the respective intraoperative MR datasets D_i of nine patients (P_1: roof of fourth ventricle – P_2: junction between pons and mid-brain – P_{3-8}: most frontal, occipital and rostral points of both lateral ventricles – P_{9-10}: locations of maximal cortex shift – $P_{11,12}$: distances in the resection area)

Data	D1	D2	D3	D4	D5	D6	D7	D8	D9
P_1	0.97	0.97	1.15	0.98	0.97	0.97	0.0	0.64	0.0
P_2	0.98	0.0	1.37	0.97	2.75	1.14	1.38	0.45	0.49
P_3	0.97	2.18	3.09	1.69	1.38	0.12	0.0	0.45	0.0
P_4	3.42	2.39	2.76	10.24	3.24	0.97	0.0	0.63	0.0
P_5	2.39	3.20	2.39	0.19	1.94	1.38	1.21	0.0	0.69
P_6	1.77	9.33	1.48	1.68	0.97	1.38	0.98	1.15	0.64
P_7	1.38	0.0	0.75	0.98	0.89	0.0	1.38	0.73	0.49
P_8	4.98	1.38	3.29	5.11	2.18	3.10	1.79	3.36	0.49
P_9	6.40	11.85	4.80	9.00	5.26	1.46	0.0	5.62	1.96
P_{10}	6.18	9.81	1.25	8.43	23.46	0.0	0.0	9.10	1.76
P_{11}	3.45	8.48	2.10	2.97	17.12	21.36	0.98	6.35	0.98
P_{12}	2.18	3.24	1.95	2.63	2.35	24.99	0.0	2.18	1.09
RMS	3.48	5.98	2.46	4.86	8.70	9.57	0.93	3.81	0.94
VAR	3.94	17.91	1.31	12.69	52.90	75.43	0.49	8.68	0.41
STD	1.98	4.23	1.15	3.56	6.73	8.32	0.70	2.73	0.64

The measurements for each patient were further analyzed with the root mean squared error (RMS), the variance (VAR) and the standard deviation (STD).

Table 6
Quality of the registration with piecewise linear transformation (refinement level III) depicted with distances (mm) between corresponding points P_i of the transformed preoperative and the respective intraoperative dataset (upper rows)

Data	D1	D2	D3	D4	D5	D6	D7	D8	D9
P_1	0.98	0.97	0.98	0.97	0.97	1.95	0.0	1.32	0.0
	−0.01	0.00	0.17	0.01	0.00	−0.98	0.00	−0.68	0.00
P_2	1.12	2.18	0.0	1.38	2.39	1.40	0.97	0.40	0.49
	−0.14	−2.18	1.37	−0.41	0.36	−0.26	0.41	0.05	0.00
P_3	0.97	2.18	1.21	0.97	1.38	0.13	0.00	0.00	0.00
	0.00	0.00	1.99	0.72	0.00	−0.01	0.00	0.45	0.00
P_4	2.65	1.74	1.08	5.78	2.39	0.98	0.00	0.00	0.00
	0.77	0.65	1.68	4.46	0.85	−0.01	0.00	0.63	0.00
P_5	0.98	1.62	1.38	0.19	1.00	1.38	1.21	0.00	1.00
	1.41	1.58	1.01	0.00	0.94	0.00	0.00	0.00	−0.31
P_6	0.00	0.00	1.48	1.68	0.97	0.00	0.97	0.12	0.64
	1.77	9.33	0.00	0.00	0.00	1.38	0.01	1.03	0.00
P_7	1.38	0.00	0.75	0.00	0.89	0.00	0.97	0.00	0.49
	0.00	0.00	0.00	0.98	0.00	0.00	0.41	0.73	0.00
P_8	1.38	2.03	2.46	0.00	1.79	0.98	0.30	0.00	0.00
	3.60	−0.65	0.83	5.11	0.39	2.12	1.49	3.36	0.00
P_9	1.38	1.50	2.18	1.54	1.46	1.46	0.00	1.00	1.40
	5.02	10.35	2.62	7.46	3.80	0.00	0.00	4.62	0.56
P_{10}	1.38	0.00	0.72	0.99	8.79	0.00	0.00	1.62	0.49
	4.80	9.81	0.53	7.44	14.67	0.00	0.00	7.48	1.27
P_{11}	0.69	2.04	0.00	1.54	1.38	1.96	0.00	1.35	0.48
	2.76	6.44	2.10	1.43	15.74	19.40	0.98	5.00	0.50
P_{12}	0.49	1.17	0.49	0.49	0.73	0.97	0.00	0.45	0.97
	1.69	2.07	1.46	2.14	1.62	24.02	0.00	1.73	0.12
RMS	1.24	1.53	1.28	1.96	2.92	1.14	0.60	0.79	0.66
VAR	0.40	0.74	0.58	2.35	4.86	0.55	0.25	0.39	0.21
STD	0.64	0.86	1.08	1.53	2.21	0.74	0.50	0.63	0.46

For comparison the magnitudes of displacements are also given (lower rows). The 9 pairs of datasets and the selected points are identical to those applied in Table 5. The measurements for each patient were further analyzed with the root mean squared error (RMS), the variance (VAR) and the standard deviation (STD).

ising, there is still work to be done considering the encountered performance limitations. For the future, it is envisaged to evaluate the integration of other modalities, such as functional data, and to extend the approach to more complex transformations.

Acknowledgements

This work was partially funded by the Deutsche Forschungsgemeinschaft (DFG) in the context of project Gr 796/2-1/2/3.

References

Arbel, T., Morandi, X., Comeau, R., Collins, D., 2001. Automatic non-linear MRI-ultrasound registration for the correction of intraoperative brain deformations. In: Proceedings of the MICCAI, Lecture Notes in Computer Science. Springer, Berlin, pp. 913–922.

Audette, M., Siddiqi, K., Peters, T., 1999. Level-set surface segmentation and fast cortical range image tracking for computing intrasurgical deformations. In: Proceedings of the MICCAI, Lecture Notes in Computer Science. Springer, Berlin, pp. 788–797.

Bier, E., Stone, M., Pier, K., 1997. Enhanced illustration using magic lens filters. IEEE Comput. Graphics Appl. 17 (6), 62–70.

Black, P., Moriarty, T., Alexander III, E., Stieg, P., Woodard, E., Gleason, P., Martin, C., Kikinis, R., Schwartz, R., Jolesz, F., 1997. Development and implentation of intraoperative magnetic resonance imaging and its neurosurgical applications. Neurosurgery 41, 831–845.

Braun, V., Dempf, S., Tomczak, R., Wunderlich, A., Weller, R., Richter, H., 2000. Functional cranial neuronavigation. Direct integration of fMRI and PET data. J. Neuroradiol. 27 (3), 157–163.

Bro-Nielsen, M., Cotin, S., 1996. Real-time volumetric deformable models for surgery simulation using finite elements and condensation. Proc. Eurograph. Comput. Graphics Forum 15 (3), 57–66.

Bucholz, R., Yeh, D., Trobaugh, J., McDurmont, L., Sturm, C., Baumann, C., Hendersonand, J., Levy, A., Kessman, P., 1997. The correction of stereotactic inaccuracy caused by brain shift using an intraoperative ultrasound device. In: Proceedings of the CVRMed-MRCAS, Lecture Notes in Computer Science. Springer, Berlin, pp. 459–466.

Cabral, B., Cam, N., Foran, J., 1994. Accelerated volume rendering and tomographic reconstruction using texture mapping hardware. ACM Symp. on Vol. Vis., 91–98.

Chabrerie, A., Ozlen, F., Nakajima, S., Leventon, M., Atsumi, H., Grimson, E., Keeve, E., Helmers, S., Riviello, J., Holmes, G., Duffy, F., Jolesz, F., Kikinis, R., Black, P., 1997. Three-dimensional reconstruction and surgical navigation in pediatric epilepsy surgery. Pediat. Neurosur. 27, 304–310.

Christensen, G., Rabbit, R., Miller, M., 1996. Deformable templates using large deformation kinematics. IEEE Trans. Image Process. 18, 875–884.

Collignon, A., Vandermeulen, D., Suetens, P., Marchal, G., 1995. Automated multi-modality image registration based on information theory. Comput. Imag. Vis. 3, 263–274.

Comeau, R., Sadikot, A., Fenster, A., Peters, T., 2000. Intraoperative ultrasound for guidance and tissue shift correction in image-guided neurosurgery. Med. Phys. 27, 787–800.

D'Agostino, E., Maes, F., Vandermeulen, D., Suetens, P., 2002. A viscous fluid model for multimodal non-rigid image registration using mutual information. In: Suresh, K. (Ed.), Proceedings of the MICCAI, Lecture Notes in Computer Science. Springer, Berlin, pp. 541–548.

Dorward, N., Alberti, O., Velani, B., Gerritsen, F., Harkness, W., Kitchen, N., Thosmas, D., 1998. Postimaging brain distortion: magnitude, correlates, and impact on neuronavigation. Neurosurgery 88, 656–662.

Fahlbusch, R., Nimsky, C., Ganslandt, O., Steinmeier, R., Buchfelder, M., Huk, W., 1998. The erlangen concept of image guided surgery. In: Proceedings of the CAR'98. Elsevier Science, Amsterdam, pp. 583–588.

Ferrant, M., Warfield, S., Nabavi, A., Kikinis, F. Jolesz R. 2000. Registration of 3D intraoperative MR images of the brain using a finite element biomechanical model. In: Suresh, K. (Ed.), Proceedings of the MICCAI, Lecture Notes in Comput Science. Springer, Berlin, pp. 19–28.

Ferrant, M., Nabavi, A., Macq, B., Jolesz, F.A., Kikinis, R., Warfield, S.K., 2001. Registration of 3-D intraoperative MR images of the brain using a finite-element biomechanical mode. IEEE Trans. Med. Img. 20 (12), 1384–1397.

Ferrant, M., Nabavi, A., Macq, B., Black, P., Jolesz, F., Kikinis, R., Warfield, S., 2002. Serial registration of intraoperative MR images of the brain. Med. Image Anal. 6 (2), 337–359.

Ganslandt, O., Steinmeier, R., Kober, H., Vieth, J., Kassubek, J., Romstöck, J., Strauss, C., Fahlbusch, R., 1997. Magnetic source imaging combined with image-guided frameless stereotaxy: A new method in surgery around the motor strip. Neurosurgery 41, 621–628.

Ganslandt, O., Fahlbusch, R., Nimsky, C., Kober, H., Möller, M., Steinmeier, R., Romstöck, Vieth, J., 1999. Functional neuronavigation with magnetoencephalography: Outcome in 50 patients with lesions around the motor cortex. J. Neurosurg. 91 (1), 73–79.

Gobbi, D., Comeau, R., Peters, T., 2000. Ultrasound/MRI overlay with image warping for neurosurgery. In: Proceedings of the MICCAI, Lecture Notes in Computer Science. Springer, Berlin, pp. 106–114.

Hagemann, A., Rohr, K., Stiehl, H.S., Spetzger, U., Gilsbach, J.M., 1999a. Biomechanical modeling of the human head for physically based, nonrigid image registration. IEEE Trans. Med. Img. 18 (10), 875–884.

Hagemann, A., Rohr, K., Stiehl, H., Spetzger, U., Gilsbach, J., 1999b. Nonrigid matching of tomographic images based on a biomechanical model of the human head. In: Hanson, K. (ed), Proceedings of the Medical Imaging – Image Processing (MI'99), pp. 583–592.

Hagemann, A., Rohr, K., Stiehl, H.S., 2000. Biomechanically based simulation of brain deformations for intraoperative image correction: coupling of elastic and fluid models. In: Medical Imaging 2000 – Image Processing (MI'2000), Proceedings of the SPIE International Symposium.

Hagemann, A., Rohr, K., Stiehl, H., 2002. Coupling of fluid and elastic models for biomechanical simulations of brain deformations using FEM. Med. Image Anal. 6 (4), 375–388.

Hall, W., Lui, H., Martin, A., Pozza, C., Truwit, R., Maxwell, C., 2000. Safety, efficacy, and functionality of high-field strength interventional magnetic resonance imaging for neurosurgery. Neurosurgery 46, 632–642.

Hartkens, T., Hill, D.., Castellano-Smith, A., Hawkes, D., Maurer Jr., C., Martin, A., Hall, W., Liu, H., Truwit, C., 2003. Measurement and analysis of brain deformation during neurosurgery. IEEE Trans. Med. Img. 22, 82–92.

Hastreiter, P., Ertl, T., 1998. Integrated registration and visualization of medical image data. In: Proceedings of the CGI, pp. 78–85.

Hastreiter, P., Rezk-Salama, C., Tomandl, B., Eberhardt, K., Ertl, T., 1998. Fast analysis of intracranial aneurysms based on interactive direct volume rendering and CT-angiography. In: Proceedings of the MICCAI, Lecture Notes in Computer Science. Springer, Berlin, pp. 660–669.

Hastreiter, P., Rezk-Salama, C., Nimsky, C., Lürig, C., Greiner, G., Ertl, T., 2000. Registration techniques for the analysis of the brain shift in neurosurgery. Comput. Graphics 24 (3), 385–389.

Hata, N., Nabavi, A., Wells III, W., Warfield, S., Kikinis, R., Black, P., Jolesz, F., 2000. Three dimensional optical flow method for measurement of volumetric brain deformation from intraoperative MR images. J. Comput Assist. Tomogr. 24, 531–538.

Hellier, P., Barillot, C., 2003. Coupling dense and landmark-based approaches for nonrigid registration. IEEE Trans. Med. Img. 22 (3), 212–217.

Hill, D., Maurer, C., Wang, M., Maciunas, R., Barwise, J., Fitzpatrick, J. 1997. Estimation of intraoperative brain surface movement. In: Proceedings of the CVRMed-MRCAS, Lecture Notes in Computer Science. Springer, Berlin, pp. 449–458.

Hill, D., Maurer, C., Maciunas, R., Barwise, J., Fitzpatrick, M., Wang, M., 1998. Measurement of intraoperattive brain surface deformation under a craniotomy. Neurosurgery 43 (3), 514–528.

Hill, D., Maurer, C., Martin, A., Sabanathan, S., Hall, W., Hawkes, D., Rueckert, D., Truwit, C. 1999. Assessment of intraoperative brain deformation using interventional MR imaging. In: Proceeding of the MICCAI, Lecture Notes in Computer Science, vol. 1679. Springer, Berlin, pp. 910–919.

Jödicke, A., Deinsberger, W., Erbe, H., Kriete, A., Böker, D., 1998. Intraoperative three-dimensional ultrasonography: An approach to register brain shift using multidemsional image processing. Minim. Invas. Neurosurg. 41, 13–19.

Kaus, M., Steinmeier, R., Sporer, T., Fahlbusch, O., Ganslandt, R., 1997. Technical accuracy of a neuronavigation system measured with a high-precision mechanical micromanipulator. Neurosurgery 41 (6), 1431–1437.

King, A., Blackall, J., Penny, G., Edwards, P., Hill, D., Hawkes, D. 2000. Bayesian estimation of intraoperative deformation for image guided surgery using 3D ultrasound. In: Proceedings of the MICCAI, Lecture Notes in Computer Science. Springer, Berlin, pp. 588–597.

Knauth, M., Wirtz, C., Tronnier, V., Staubert, A., Kunze, S., Sartor, K., 1998. Intraoperative Magnetresonanztomographie zur Radikalitatskontrolle bei neurochirurgischen Operationen. Radiologe 38, 218–224.

Kyriacou, S., Davatzikos, C. 1998. A biomechanical model of soft tissue deforamtion with applciations to non-rigid registration of brain images with tumor pathology. In: Proceedings of the MICCAI, Lecture Notes in Computer Science, vol. 1496. Springer, Berlin, pp. 531–538.

Kyriacou, S., Shen, D., Davatzikos, C. 2000. A framework for predictive modeling of intra-operative deformations: A simulation-based study. In: Proceedings of the MICCAI, Lecture Notes in Computer Science, vol. 1935. Springer, Berlin, pp. 634–642.

Lester, H., Arridge, S., Janson, K., 1998. Local deformation metrics and nonlinear registration using a fluid model with variable viscosity. In: Berry, E., Hogg, D., Mardia, K., Smith, M. (eds), Proceedings of the Medical Image Understanding and Analysis (MIUA), pp. 44–48.

Levivier, M., Goldmann, S., Pirotte, B., Brucher, J., Baleriaux, D., Luxen, A., Hildebrand, J., Brotchi, J., 1995. Diagnostic yield of stereotactic brain biopsy by positron emission tomography with [^{18}F]fluorodeoxyglucose. J. Neurosurg. 82, 445–452.

Lunsford, L., Parrish, R., Albright, L., 1984. Intraoperative imaging with a therapeutic computed tomographic scanner. Neurosurgery 15, 559–561.

Lürig, C., Kobbelt, L., Ertl, T., 1998. Deformable surfaces for feature based indirect volume rendering. In: Proceedings of the Computer Graphics International (CGI), pp. 752–760.

Maciunas, R., Galloway, R., Latimer, J., 1994. The application accuracy of stereotactic frames. Neurosurgery 35, 682–695.

Maes, F., Collignon, A., Vandermeulen, D., Marchal, G., Suetens, P., 1997. Multimodality image registration by maximization of mutual information. IEEE Trans. Med. Img. 16 (2), 187–198.

Maurer, C., Hill, D., Martin, A., Liu, H., McCue, M., Rueckert, D., Lloret, D., Hall, W., Maxwell, R., Hawkes, D., Truwit, C., 1998. Investigation of intraoperative brain deformation using a 1,5 T interventional MR system: preliminary results. IEEE Trans. Med. Img. 17 (5), 817–825.

Miga, M., Staubert, A., Paulsen, K., Tronnier, F., Kennedy, V., Roberts, D., 1999. Model updated image guidance: Initial clinical experiences with gravity-induced brain deformation. IEEE Trans. Med. Img. 18, 866–874.

Miga, M., Paulsen, K., Hoopes, P., Kennedy, F., Hartov, A., Roberts, D., 2000a. In-vivo analysis of heterogeneous brain deformation computations for model-updated image guidance. Comput. Meth. Biomech. Biomed. Eng. 3, 129–146.

Miga, M., Paulsen, K., Hoopes, P., Kennedy, F., Hartov, A., 2000b. In vivo modeling if intersitial pressure in the brain under surgical load using finite elements. J. Biomech. Eng. 122, 354–363.

Miga, M., Paulsen, K., Hoopes, P., Kennedy, F., Hartov, A., Roberts, D., 2000c. In vivo quantification of a homogeneous brain deformation model for updating preoperative images during surgery. IEEE Trans. Biomed. Eng. 47 (2), 266–273.

Miga, M., Staubert, A., Paulsen, K., Kennedy, F., Tronnier, V., Roberts, D., Hartov, A. 2000d. Model-updated image-guided neurosurgery: preliminary analysis using intraoperative MR. In: Proceedings of the MICCAI, Lecture Notes in Computer Science. Springer, Berlin, pp. 115–124.

Nabavi, A., Hata, N., Gering, D., Chatzidakis, E., Leventon, M., Weisenfeld, N., Pergolizzi, R., Oge, K., Black, P., Jolesz, F., Kikinis, R. 1999. Image guided neurosurgery: visualization of brain shift. In: Spetzger, U., Stiehl, S., Gilsbach, J. (Eds), Proceedings of the Navigated Brain Surgery. Verlag Mainz, Aachen, pp. 17–26.

Nabavi, A., Black, P., Gering, D., Westin, C., Mehta, V., Pergolizzi, R., Ferrant, M., Warfield, S., Hata, N., Schwartz, R., Wells III, W., Jolesz, R., Kikinis, F., 2001. Serial intraoperative magnetic resonance imaging of brain shift. Neurosurgery 48 (4), 787–797.

Nakajima, S., Atsumi, H., Kikinis, R., Moriarty, T., Metcalf, D., Jolesz, F., Black, P., 1997. Use of cortical surface vessel registration for image-guided neurosurgery. Neurosurgery 40 (6), 1201–1210.

Nimsky, C., Ganslandt, O., Kober, H., Möller, M., Ulmer, S., Tomandl, B., Fahlbusch, R., 1999. Integration of functional magnetic resonance imaging supported by magnetoencephalography in functional neuronavigation. Neurosurgery 44, 1249–1256.

Nimsky, C., Ganslandt, O., Cerny, S., Hastreiter, P., Greiner, G., Fahlbusch, R., 2000. Quantification of, visualization of, and compenstation for brain shift by intraoperative magnetic resonance imaging. Neurosurgery 47 (5), 1070–1080.

Nimsky, C., Ganslandt, O., Hastreiter, P., Fahlbusch, R., 2001a. Intraoperative compensation for brain shift. Surg. Neurol. 56 (6), 357–364.

Nimsky, C., Ganslandt, O., Kober, H., Buchfelder, M., Fahlbusch, R., 2001b. Intraoperative magnetic resonance imaging combined with neuronavigation: a new concept. Neurosurgery 48 (5), 1082–1089.

Nimsky, C., Ganslandt, O., Buchfelder, M., Fahlbusch, R., 2003. Glioma surgery evaluated by intraoperative low-field magnetic resonance imaging. Acta Neurochir. Suppl 85, 55–63.

Ourselin, S., Stefanescu, R., Pennec, X. 2002. Robust Registration of multi-modal images: towards real-time clinical applications. In: Proceedings of the MICCAI, Lecture Notes in Computer Science. Springer, Berlin, pp. 140–147.

Paulsen, K., Miga, M., Kennedy, F., Hoopes, P., Hartov, A., Roberts, D., 1999. A computational model for tracking subsurface tissue deformation during stereotactic neurosurgery. IEEE Trans. Biomed. Eng. 46, 213–225.

Porter, T., Duff, T., 1984. Compositing digital images. In: Proceedings of the SIGGRAPH, Computer Graphics Conference Series, pp. 253–259.

Press, W., Flannery, B., Teukolsky, S., Vetterling, W., 1988. Numerical Recipes in C. Cambridge University Press, Cambridge.

Rezai, A., Hund, M., Kronberg, E., Zonenshayn, M., Cappell, J., Ribary, U., Kall, B., Llinas, R., Kelly, P., 1996. The interactive use of magnetoencephalography in stereotactic image-guided neurosurgery. Neurosurgery 39 (1), 92–102.

Rezk-Salama, C., Engel, K., Bauer, M., Greiner, G., Ertl, T., 2000. Interactive volume rendering on standard pc graphics hardware using multi-textures and multi-stage rasterization. In: Proceedings of the Eurographics/SIGGRAPH Workshop on Graphics Hardware.

Rezk-Salama, C., Scheuering, M., Soza, G., Greiner, G. 2001. Fast volumetric deformation on general purpose hardware. In: Proceedings of the SIGGRAPH/Eurographics Workshop on Graphics Hardware.

Roberts, D., Hartov, A., Kennedy, F., Miga, M., Paulsen, K., 1998. Intaoperative brain shift and deformation: a quantitative analysis of cortical displacement in 28 cases. Neurosurgery 43 (4), 749–760.

Roberts, D., Miga, M., Hartov, A., Eisner, S., Lemery, J., Kennedy, F., Paulsen, K., 1999. intraoperatively updated neuroimaging using modeling and sparse data. Neurosurgery 45, 1199–1207.

Roberts, T., Zusman, E., McDermott, M., Barbaro, N., Rowley, H., 1995. Correlation of functional magnetic source imaging with intraoperative cortical stimulation in neurosurgical patients. J. Image Guid. Surg. 1 (6), 339–347.

Rohlfing, T., Maurer Jr., C., 2003. Nonrigid image registration in shared-memory multiprocessor environments with application to brains, breasts, and bees. IEEE Trans. Med. Img. 22 (6), 730–741.

Rohlfing, T., Maurer Jr, C., Bluemke, D., Jacobs, M., 2003. Volume-preserving nonrigid registration of MR breast images using free-form deformation with an incompressibility constraint. IEEE Trans. Med. Img. 22 (6), 730–741.

Samset, E., Hirschberg, H., 1999. Neuronavigation in Intraoperative MRI. Comput. Aided Surg. 4, 200–207.

Schnabel, J., Rueckert, D., Quist, M., Blackall, J., Castellano-Smith, A., Hartkens, T., Penney, G., Hall, W., Liu, H., Truwit, C., Gerritsen, F., Hill, D., Hawkes, D. 2001. A generic framework for non-rigid registration based on non-uniform multi-level free-form deformations. In: Proceedings of the MICCAI, Lecture Notes in Computer Science. Springer, Berlin. pp. 573–581.

Schnabel, J., Tanner, C., Castellano-Smith, A., Degenhard, A., Leach, M., Hose, D., Hill, D., Hawkes, D., 2003. Validation of nonrigid image registration using finite-element methods: application to breast MR images. IEEE Trans. Med. Img. 22, 238–247.

Skrinjar, O., Duncan, J. 1999. Real time 3d brain shift compensation. In: Kuba, A., Samal, M., Todd-Pokropek, A. (Eds.), Proceedings of the Information Processing in Medical Imaging (IPMI). Springer, Berlin, pp. 42–55.

Skrinjar, O., Nabavi, A., Duncan, J., 2002. Model-driven brain shift compensation. Med. Image Anal. 6 (4), 361–373.

Steinmeier, R., Fahlbusch, R., Ganslandt, O., Nimsky, C., Buchfelder, M., Kaus, M., Heigl, T., Lenz, G., Kuth, R., Huk, W., 1998. Intraoperative magnetic resonance imaging with the magnetom open scanner: concepts, neurosurgical indications, and procedures. A preliminary report. Neurosurgery 43, 739–748.

Studholme, C., Hill, D., Hawkes, D., 1996. Automated 3D registration of truncated MR and CT images of the head. In: Proceedings of the British Mach. Visual Conference (BMVC).

Studholme, C., Hill, D., Hawkes, D., 1999. An overlap invariant entropy measure of 3D medical image alignment. Pattern Recogn. 32, 71–86.

Sutherland, G., Kaibara, T., Louw, D., Hoult, D., Tomanek, B., Saunders, J., 1999. A mobile high-field magnetic resonance system for neurosurgery. Neurosurgery 91, 804–813.

Tomandl, B., Hastreiter, P., Rezk-Salama, C., Engel, K., Ertl, T., Huk, W., Ganslandt, O., Nimsky, C., Eberhardt, K., 2001. Local and remote visualization techniques for interactive direct volume rendering in neuroradiology. RadioGraphics 21, 1561–1572.

Tronnier, V., Wirtz, C., Knauth, M., Lenz, G., Pastyr, O., Bonsanto, M., Albert, F., Kuth, R., Staubert, A., Schlegel, W., Sartor, K., Kunze, S., 1997. Intraoperative diagnostic and interventional magnetic resonance imaging in neurosurgery. Neurosurgery 40, 891–900.

Viega, J., Conway, M., Williams, G., Pausch, R., 1996. Magic Lenses.

Wells, W., Viola, P., Kikinis, R., 1995. Multi-modal volume registration by maximization of mutual information. Proc. Med. Robot. Comput Assis. Surg., 55–62.

West, J., Fitzpatrick, J.M., Wang, M.Y., Dawant, B.M., Maurer Jr., C., Kessler, R.M., Maciunas, R.J., 1999. Retrospective intermodality registration techniques for images of the head: surface-based versus volume-based. IEEE Trans. Med. Img. 18 (2), 144–150.

Wirtz, R., Bonsanto, M., Knauth, M., Tronnier, V., Albert, F., Staubert, A., Kunze, S., 1997. Intraoperative magnetic resonance imaging to update interactive navigation in neurosurgery: methode and preliminary experience. Comput. Aid. Surg. 2, 172–179.

Wollny, G., Kruggel, F., 2002. Computional cost of nonrigid registration algorithms based on fluid dynamics. IEEE Trans. Med. Img. 21 (8), 946–952.